EUROPEAN ORGANIZATION FOR NUCLEAR RESEARCH

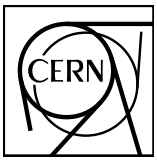

CERN-PH-EP-2015-XXX
Day Month 2015

Λ and K^0_S production in jets in p–Pb collisions at $\sqrt{s_{NN}} = 5.02$ TeV

ALICE Collaboration*

Abstract

To sched light on the origin of the so-called "baryon enhancement" observed in p–Pb collisions at $\sqrt{s_{NN}} = 5.02$ TeV at the LHC the production of Λ baryons and K^0_S mesons was measured separately in hard scattering region and the underlying event. The hard scatterings are selected on an event-by-event basis by jets reconstructed using charged particles with anti$-k_T$ jet finder. The production of strange particles is reported as a function of their transverse momentum p_T and the angular distance R from the jet axis for jets with $p_{T\,ch\,jet} > 10$ GeV/c and $p_{T\,ch\,jet} > 20$ GeV/c.

For small R ($R < 1.0$) the $(\Lambda+\overline{\Lambda})/K^0_S$ ratio associated to jets is found consistent with the expectation of jets fragmenting in vacuum given by PYTHIA event generator. In contrast, this ratio for large R corresponding to the underlying event shows a maximum similar to that of inclusive production in p–Pb collisions at the intermediate p_T of 2-5 GeV/c.

*See Appendix A for the list of collaboration members

1 Introduction

High-energy heavy ion collisions provide a unique opportunity to study properties of hot and dense QCD medium composed of deconfined partons - the quark-gluon plasma (QGP). The QGP is predicted by the lattice QCD calculations [1–4]. The cross-over transition from hadronic matter to the QGP matter at zero baryochemical potential is expected to take place once the temperature of the matter T_c reaches values of about 150 MeV and/or energy density ε_c of about 0.5 GeV/fm^3 [5, 6]. The measurements indicate that the most violent collisions of lead ions at the Large Hadron Collider (LHC) at centre-of-mass energy per nucleon-nucleon collision $\sqrt{s_{\rm NN}} = 2.76$ TeV create conditions well above the critical temperature at approximately zero baryochemical potential. The bulk matter created in those collisions can be quantitatively described in terms of relativistic hydrodynamics and statistical hadronization models. The initial hot and dense partonic matter rapidly expands and cools down, ultimately undergoing a transition to a hadron gas phase [7]. During the expansion phase, collective hydrodynamic flow develops from the initially generated pressure gradients in the strongly interacting system. This results in a characteristic dependence of the shape of the transverse momentum ($p_{\rm T}$) distribution on the particle mass that can be described using a common kinetic freeze-out temperature parameter $T_{\rm kin}$ and a collective average expansion velocity $\langle\beta_{\rm T}\rangle$ [8].

The interpretation of heavy-ion results depends on the understanding of results from smaller collision systems such as proton-proton (pp) or proton-nucleus (pA). Comparisons of particle production in pp, pA, and AA reactions has frequently been used to separate initial state effects, linked to the use of nuclear beams or targets, from final state effects, associated to the presence of hot and dense matter. However, the measurements at the LHC in high-multiplicity pp and p–Pb collisions have revealed unexpectedly strong long-range correlations of produced particles [9–14] falsifying the assumption that final state effects can be neglected in pA. Moreover, measurements of identified hadron production [15] have shown qualitatively similar features as in AA collisions [16, 17]. In particular, the ratio of baryon and meson transverse momentum ($p_{\rm T}$) spectra shows a pronounced maximum at intermediate (2-5 GeV/c) $p_{\rm T}$ [15]. The $p_{\rm T}$ dependence of the ratio has been discussed in terms of an interplay between the radial expansion of the system and particle production within a common velocity field (collective flow) [8], soft-hard parton recombination [18] and high energy parton shower (jet) hadronization at high $p_{\rm T}$. On the other hand, the measurements of inclusive jet production at mid-rapidty in pA collisions [19, 20] show that the final state nuclear effects such as shadowing and gluon saturation (CGC) [21, 22], or multiple scatterings and hadronic re-interactions in the initial and final state [23, 24] are negligible as compared to the same measurements in pp collisions. In particular, the suppression related to the creation of the QGP in AA collisions was not observed in p–Pb collisions [25–29].

In this letter we report on the measurement of Λ, $\overline{\Lambda}$ and $\rm K^0_S$ where their production is studied separately within the region associated to a hard scattering and the remainder of the event (the so called "underlying event"). The hard scatterings are tagged by selecting a jet ($p_{\rm T}^{\rm jet} > 10$ or 20 GeV/c) reconstructed using charged particles with the anti-$k_{\rm T}$ algorithm with the resolution parameter $R = 0.2$, 0.3 and 0.4. The $\Lambda/\rm K^0_S$ ratio associated to jets is reported as a function of particle momentum and as a function of their distance to the jet axis.

2 Data analysis

2.1 Data sample and detector description

The data used in this analysis was recorded by the ALICE detector [30] during the LHC p–Pb run at $\sqrt{s_{\rm NN}} = 5.02$ TeV in the beginning of 2013. Since the "two-in-one" magnet design of the LHC [31], the energies of the two beams are not independent and their ratio is fixed to equal to the ratio of the charge/mass ratios of each beam. Consequently, the nucleon-nucleon center-of-mass system (cms) was shifted by a rapidity of $\Delta y_{\rm NN} = 0.465$ in the direction of the proton beam. The analyzed data was collected for the beam configuration, in which the Pb beam circulated in the "counter-clockwise" direction traveling from negative to positive rapidity.

The ALICE apparatus described in detail in [30] consists of central barrel detectors covering the pseudo-rapidity interval $|\eta_{\rm lab}| < 0.9$, a forward muon spectrometer covering $-4.0 < \eta_{\rm lab} < -2.5$, and a set of detectors at forward and backward rapidities used for triggering and event characterization. The data presented in this letter were recorded using the minimum bias trigger provided by the V0 detector system [32] consisting of two arrays of 32 scintillator tiles each, placed around the beam vacuum tube on either side of the interaction region covering the pseudo-rapidity intervals $2.8 < \eta_{\rm lab} < 5.1$ (V0A) and $-3.7 < \eta_{\rm lab} < -1.7$ (V0C). A coincidence of signals in both V0A and V0C was required to remove contamination from single diffractive and electromagnetic events [33]. In addition two neutron Zero Degree Calorimeters (ZDCs) located at +112.5 m (ZNA) and −112.5 m (ZNC) from the interaction point were used for beam background rejection. A dedicated quartz radiator Cherenkov detector (T0) [34] provided the measurement of the event time of the collision.

Tracking and particle identification were performed using the information provided by the Inner Tracking System (ITS) [35], the Time Projection Chamber (TPC) [36] and the Time Of Flight (TOF) [34] detectors, that have full azimuthal coverage in the pseudo-rapidity interval $|\eta_{\rm lab}| < 0.9$. These central barrel detectors are located inside a large solenoidal magnet, which provides a magnetic field of 0.5 T along the beam direction (z axis in the ALICE reference frame).

The ITS is composed of six cylindrical layers of silicon detectors, with radial distances from the beam axis ranging from 3.9 cm to 43.0 cm. The two innermost layers, with average radii of 3.9 cm and 7.6 cm, are equipped with Silicon Pixel Detectors (SPD) covering the pseudo-rapidity ranges of $|\eta_{\rm lab}| < 2.0$ and $|\eta_{\rm lab}| < 1.4$ respectively. The two intermediate layers are made of Silicon Drift Detectors (SDD), while Silicon Strip Detectors (SSD) equip the two outermost layers. The high spatial resolution of the silicon sensors, together with the low material budget (on average 7.7% of a radiation length for tracks crossing the ITS perpendicularly to the detector surfaces, i.e. $\eta_{\rm lab} = 0$) and the small distance of the innermost layer from the beam vacuum tube, allow for the measurement of the track impact parameter $d_{\rm DCA}$ in the transverse plane. The $d_{\rm DCA}$ is defined by the distance of closest approach (DCA) of the track to the primary vertex in the plane transverse to the beam direction, and is measured with a resolution better than 75 μm for transverse momenta $p_{\rm T} > 1$ GeV/c [35]. The events were further selected by requiring a reconstructed vertex within 10cm ($v_z < 10$cm) along beam axis and that the vertices built from SPD tracklets and from the global tracks (combining information of ITS and TPC) were compatible. The analysis required a reconstructed vertex, which was the case for 98.2% of the events selected by the trigger. The total number of events retained in the analysis was $96 \cdot 10^6$.

At larger radii ($85 < r < 247$ cm), a 510 cm long cylindrical TPC provides track reconstruction

with up to 159 three-dimensional space points per track, as well as particle identification via the measurement of the specific energy deposit $\mathrm{d}E/\mathrm{d}x$ in the gas. The charged particle identification capability of the TPC is supplemented by the TOF, which is equipped with Multi-gap Resistive Plate Chambers (MRPCs) located at radial distances between 377 and 399 cm from the beam axis. The overall TOF resolution including the uncertainty on the time at which the collision took place, and the tracking and momentum resolution was about 160 ps for the data-taking period considered in this analyses.

2.2 Charged particle and jet reconstruction

The charged particle and jet reconstruction in this letter follows the analysis described in detail in [19]. Here only a brief review of the most relevant points is discussed. Charged particle tracks reconstructed in the ITS and the TPC with $p_{\mathrm{T}} > 0.15$ GeV/c and within a pseudorapidity interval $|\eta_{\mathrm{lab}}| < 0.9$ that satisfied a DCA requirement $d_{\mathrm{DCA}} < 2.4$ cm were used as input to the jet reconstruction. The azimuthal distribution of these high quality tracks is not completely uniform due to inefficient regions in the SPD. This was compensated by considering in addition tracks without reconstructed track points in the SPD. To improve the momentum resolution for those tracks, the primary vertex was used as an additional constraint in the track fitting. This approach yields a uniform tracking efficiency within the acceptance, which is needed to avoid geometrical biases in the jet reconstruction that can be caused by an unphysical non-uniform density of reconstructed tracks. The procedure is described in detail in the context of jet reconstruction in [19]. For the analyzed data, the additional tracks (without SPD track points) constitute approximately 4.3% of the used track sample. The overall efficiency for charged particle detection, including the effect of tracking efficiency as well as the geometrical acceptance, is 70% at $p_{\mathrm{T}} = 0.15$ GeV/c and increases to 85% at $p_{\mathrm{T}} = 1$ GeV/c and above.

The jets were reconstructed using the anti-k_{T} algorithm [37] from the FastJet package [38, 39] with resolution parameters of $R = 0.2$, 0.3 and 0.4. Only the jets where the jet-axis was found within the acceptance window $|\eta_{\mathrm{lab}}| < 0.35$ that is fully overlapping with the acceptances of both charged particle tracks ($|\eta_{\mathrm{lab}}| < 0.9$) and V^0s ($|\eta_{\mathrm{lab}}| < 0.75$) for any of the jet resolution parameters. The jet transverse momentum is calculated by FastJet using the p_{T} recombination scheme.

In general the transverse momentum density of the background originating from the underlying event and/or pile-up (particles not associated to the hard scattering) contributes to the jet energy reported by the jet finder. The correction of the jet energy scale accounting for the background energy can be estimated on event-by-event basis using the median of all jet candidate clusters $p_{\mathrm{T\,ch\,jet}}$ reconstructed with the k_{T} algorithm per unit area [40]. This method has been used in the analysis of Pb–Pb events [28, 41]. In this analysis, an estimate adequate for the more sparse environment of p–Pb collisions was employed [19]. The resulting mean of the background p_{T} density $\langle \rho^{\mathrm{ch}} \rangle = 1.02$ GeV/c rad^{-1} with a standard deviation of $\sigma(\rho^{\mathrm{ch}}) = 0.91$ GeV/c rad^{-1} for unbiased events and, $\langle \rho^{\mathrm{ch}} \rangle = 2.2$ GeV/c rad^{-1} and $\sigma(\rho^{\mathrm{ch}}) = 1.47$ GeV/c rad^{-1} for events containing a jet with $p^{raw}_{\mathrm{T\,ch\,jet}} > 20$ GeV/c [19].

The resulting kinematic efficiency for generator level jets was established using using PYTHIA [42]. For jets of $p_{\mathrm{T}} = 10$ GeV/c it was about 65% and 90% for jets with $p_{\mathrm{T}} = 20$ GeV/c.

2.3 Particle identification and V^0 particle reconstruction

Charged-hadron identification in the central barrel was performed with the ITS, TPC and TOF detectors. The drift and strip layers of the ITS provide a measurement of the specific energy loss with a resolution of about 10%. In a standalone tracking mode, the identification of pions, kaons, and protons is thus extended down to respectively 0.1, 0.2, 0.3 GeV/c in p_{T}. The TPC provides particle identification at low momenta via specific energy loss $\mathrm{d}E/\mathrm{d}x$ in the gas by measuring up to 159 samples per track with a resolution of about 6%. The separation power achieved in p–Pb collisions is identical to that in pp collisions [43]. Further outwards at about 3.7 m from the beam line, the TOF array allows identification at higher p_{T} measuring the particle speed with the time-of-flight technique. The total time resolution is about 85 ps for events in the multiplicity classes from 0% to $\sim$ 80%. In more peripheral collisions, where multiplicities are similar to pp, it decreases to about 120 ps due to a worse start-time (collision-time) resolution [43]. The start-time of the event was determined by combining the time estimated using the particle arrival times at the TOF and the time measured by the T0 detector.

The V^0 particles, K^0_S and Λ ($\overline{\Lambda}$), were identified exploring the characteristics of their weak decay topologies in the channels $K^0_S \rightarrow \pi^+\pi^-$ and $\Lambda(\overline{\Lambda}) \rightarrow p\pi^-(\overline{p}\pi^-)$, which have branching ratios of 69.2% and 63.9%, respectively [44]. The reconstruction and the selection criteria of the V^0 particles follow the analysis in [15] with the exception of the rapidity selection of the particles and their decay products. In particular, p_{T} differential yields of V^0particles were extracted via the invariant mass method described in [15] but the V^0 decay-product tracks were selected in the acceptance window $|\eta_{\mathrm{lab}}| < 0.8$, whereas only the V^0 candidates found in $|\eta_{\mathrm{lab}}| < 0.75$ were retained. This ensured that the reconstruction efficiency was approximately constant throughout the selected pseudo-rapidity. The topological selection of V^0 candidates within the kinematic range of this analysis yielded an almost background free invariant mass spectra with the lowest signal/background ratio among all of the V^0 particles still greater than 10. We note that due to the track selection optimized for weak decays only about 0.1% of the V^0 daughter tracks contribute to the charged particle jet reconstruction.

2.4 Matching of V^0 particles to jets and underlying event

To obtain the yield of V^0 particles within a jet cone the V^0 particles are selected based on their distance from the jet centroid $R_{\mathrm{V^0-jet}}$ in the pseudo-rapidity and azimuthal angle plane ($\eta_{\mathrm{lab}} \times \varphi$)) such that:

$$R_{\mathrm{V^0-jet}} = \sqrt{(\eta^{\mathrm{jet}}_{\mathrm{lab}} - \eta^{\mathrm{V^0}}_{\mathrm{lab}})^2 - (\varphi^{\mathrm{jet}} - \varphi^{\mathrm{V^0}})^2}. \quad (1)$$

A particle that is within the radius $R < R_{\mathrm{V^0-jet}}$ is considered matched to a given jet. In p–Pb collisions the probability for a particle with $p_T > 0.5$ GeV/c to match to two jets with $p^{\mathrm{jet}}_{\mathrm{T}} > 10$ GeV/c is significantly less than 1% and in these cases the higher energy jet is preferred. Moreover, removal of the events with two or more jets matching a single particle did not alter the result of the analysis. The procedure for extraction of the yield of V^0 particles associated with a jet within a cone R (JC V^0) can be summarized as follows. The V^0 candidates selected within the acceptance of $|\eta| < 0.75$ were associated to the hard scattering with a distance cut in pseudo-rapidity and azimuthal angle plane $R_{\mathrm{V^0-jet}} < R$. For each p_{T} interval the JC raw yield of V^0 particles was established using the invariant mass technique where the combinatorial background was interpolated from the side bands around the mass peak. The mass peak is

defined by the width and mean of the peak for the inclusive V^0 candidates. Then the raw JC yield can be corrected for the contribution of particles from the underlying event (UE). The UE is simply defined as set of particles that is not associated to the hard scatterings tagged by the charged jets considered in this analysis.

To extract the UE yield of V^0 particles several estimators have been investigated: i) the so-called *outside cone* (OC) selection composed of the V^0 particles that were not matched to any jet considered in the analysis within events containing a jet such that $R_{V^0-\mathrm{jet}} > R_{\mathrm{cut}}$; ii) the *perpendicular cones* (PC) selection composed of the V^0 particles found at azimuthal angles larger than R_{cut}: $\Delta\varphi > R_{\mathrm{cut}}$, where $\Delta\varphi = \varphi^{\mathrm{jet}} - \varphi^{V^0}$; and iii) the *non-jet events* (NJ) selection composed of the V^0 particles found in events that do not contain a jet with $p_{\mathrm{T}}^{\mathrm{jet}} > 5$ GeV/c.

In practice, a useful quantity for performing the subtraction of the non-jet contribution of the V^0 particles is their density per unit area

$$\rho^{V^0}(p_{\mathrm{T}}) = N^{V^0}(p_{\mathrm{T}})/A^{V^0}, \tag{2}$$

where N^{V^0} is the number of particles and A^{V^0} is the acceptance in pseudo-rapidity and azimuthal angle. Consequently, the number of the UE V^0 particles within a jet can be calculated as $N = \rho^{V^0} A^{\mathrm{jet}}$ for each estimator separately. In this analysis we consider the jet area $A^{\mathrm{jet}} = \pi R^2$. In general the density of V^0 particles within jets (JC) can be defined as $\rho_{\mathrm{JC}}^{V^0} = \rho_{\mathrm{JC,raw}}^{V^0} - \rho_{\mathrm{UE}}^{V^0}$, where UE can be any of the OC, PC, NJ background estimators. In this analysis we choose PC as the default background estimator and use OC and NJ to quantify the systematic uncertainty.

2.5 Corrections for finite V^0 reconstruction and feed-down

The reconstruction efficiencies of V^0 particles were estimated using DPMJET Monte Carlo generator [45] with the same cuts as in the data except the daughter track particle identification with $\mathrm{d}E/\mathrm{d}x$ in TPC (see more details in [15]). Due to differences in the experimental acceptance for V^0 particles associated to jets (JC) and those extracted through the various estimators of the underlying event (OC, PC, NJ) the efficiencies of V^0 particles were estimated separately for every case. Figure 1 shows the inclusive reconstruction efficiency for V^0 particles and the efficiency in the events containing a jet for two selections of distance R from the main jet axis. In particular, for $R(V^0, jet) < 0.4$ the efficiency at $p_{\mathrm{T}} < 2$GeV/c is about 20% greater than in the inclusive case while it approaches the inclusive case at higher p_{T}. The efficiency for events containing a jet varies moderately with R (within a 5%) and for every selection of R the efficiencies were evaluated separately.

The p_{T} differential yields of Λ and $\overline{\Lambda}$ reconstructed for each selection (JC and UE selections) were in addition also corrected for the feed-down from Ξ decays. The Ξ production in jets (JC) was estimated based on measurements of the multi-strange baryons and their decays at high-p_{T} performed in pp collisions [46] and extrapolated to the lower p_{T} using PYTHIA event generator and full detector simulations. The applied correction amounts to 15% and is independent of the Λ and $\overline{\Lambda}$ momentum. Conversely, Λ yields were not corrected for the feed-down from Ω^- baryons nor for the feed-down from non-weak decays of Ξ^0 and $\Xi(1385)$ family as these contributions are neglibible as compared to the systematic uncertainties of the present measurement.

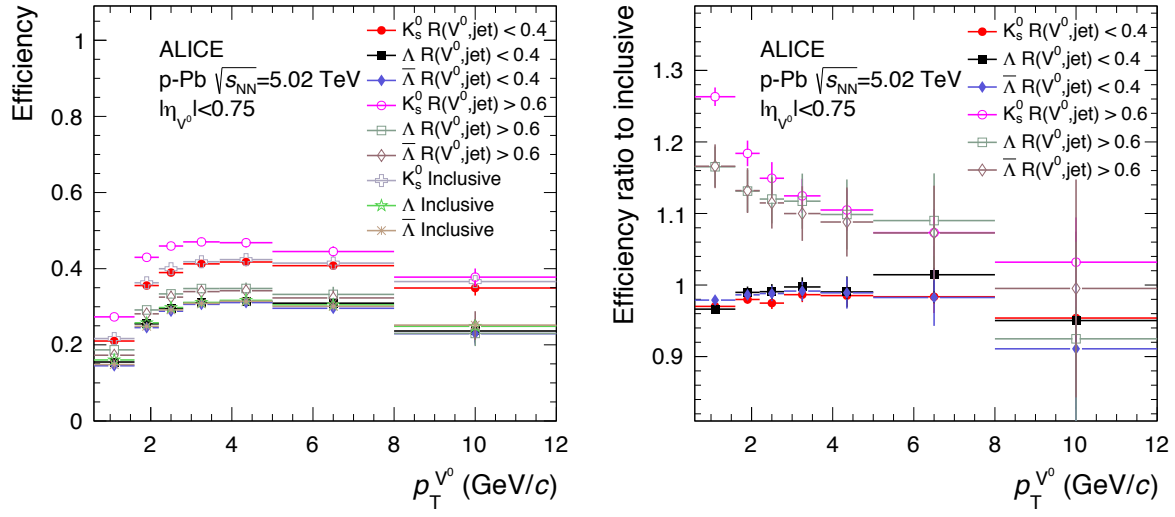

Fig. 1: Efficiency of V^0 particles in p–Pb collisions at $\sqrt{s_{NN}} = 5.02$ TeV for three selections: inclusive, within $R_{V^0-jet} < 0.4$ and $R_{V^0-jet} > 0.6$. The efficiencies for Λ (not shown) is consistent with the efficiency for $\overline{\Lambda}$ within about 5% and showing similar p_T dependence.

2.6 Systematic uncertainties

The main sources in the V^0 particle reconstruction are the level of knowledge of the detector material (resulting in a 4% uncertainty), the track selection (up to 4%), the feed-down correction for the Λ (5% for $p_T < 3.7$GeV$/c$ and 7% for $p_T > 3.7$GeV$/c$), the proper lifetime selection criteria (up to 3%) and the topological selections that contribute up to 1.5% depending on transverse momentum and particle species.

The p_T-dependent uncertainties on the extracted yields of V^0 particles are shown in Fig. 2 for K^0_S mesons and $\overline{\Lambda}$ baryons. To calculate the total uncertainty on the yields the individual uncertainties on track selection, material budged, feed-down corrections and the listed V^0 selections are added in quadrature.

Particle identification (PID). Uncertainty due to the particle identification cuts was estimated by varying the cuts on the d$E/$dx TPC from a default 5σ to 4, 6 and 7 standard deviations from the nominal d$E/$dx for pions and protons.

Track selection. Uncertainty on the V^0 yields originating from the track selection was estimated by repeating the analysis with the increased number of required TPC space points per track by about 7% and 15% from the nominal. **MP: it is very difficult to find in ALICE papers this type of definition... ;-(**

Topological selection. The uncertainty associated to topological cuts on the V^0 candidates (the two dimensional decay radius, daughter track DCA to primary vertex, minimum DCA of V^0 daughters, and maximum cosine of the pointing angle) was obtained by varying the parameters of the selections for each of the V^0 species separately as described in detail in [15].

Proper lifetime selection. The uncetainty due to the cuts on the proper lifetime of the V^0 candidates defined as the product of mass m, decay length L and the inverse of particle's mo-

mentum p ($mL/p < 20$ *cm* for K^0_S and $mL/p < 30$ *cm* for Λ baryons) was obtained by redoing the analysis with different cuts (12 and 40 *cm* for K^0_S and 20 and 40 *cm* for Λ and $\overline{\Lambda}$).

Competing V^0 selection. To obtain the uncertainty related to the cut on the competing V^0 particles defined as the absolute mass difference between V^0 candidate and the rest mass of the competing weakly decaying hadron (> 0.005 GeV$/c^2$ for K^0_S and > 0.010 GeV$/c^2$) the analysis was repeated with 3 and 6 MeV$/c^2$ for K^0_S and with no rejection for Λ baryons.

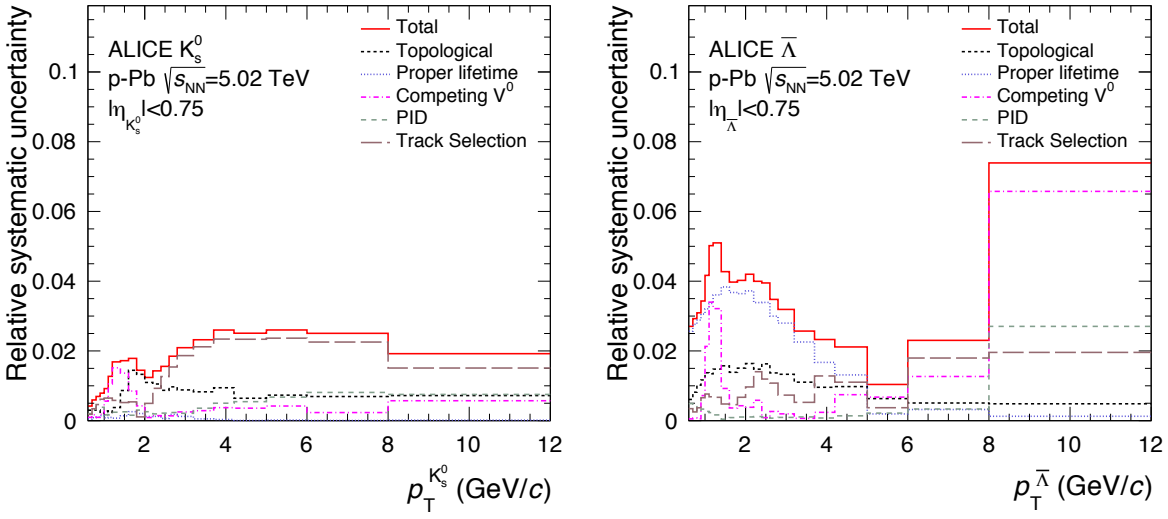

Fig. 2: Systematic uncertainties on V^0 particle spectrum (left: K^0_S, right: $\overline{\Lambda}$) as a function of their transverse momentum (see text and Tab. **??** for details). The systematic uncertainties associated to the Λ yield (not shown) are largely similar to $\overline{\Lambda}$. **MP: Uncertainties should be smoothed (local minima in some cases are unphysical).**

Uncertainty on the yields in the underlying event. Two main sources of uncertainties originating from the mis-association of V^0particles with UE were considered: i) the V^0 particle was found outside the selected jet and classified as UE particle; however, it may have originated from a physical jet outside the fiducial acceptance for jets considered in the analysis and/or from a *true* low-p_T jet, below the considered thresholds; and ii) the V^0 particle originates from a true high-p_T jet; however, due to the finite detector efficiency the jet has not been reconstructed above the considered p_T threshold.

The uncertainty on the UE V^0 density has been estimated using the two variations of the UE estimators: the *outside cone* (OC) and the *non-jet events* (NJ). The OC and the NJ estimators encapsulate the maximum deviation in the yield of UE particles and the difference of the reconstructed V^0 yields in OC and NJ has been included as the additional systematic uncertainties on the density of particles within the jets (JC). The uncerainty is largest for low-momenta particles (< 2 GeV$/c$) reaching up to 30% but drops rapidly with p_T to negligible values at 6 GeV$/c$. **check numbers** .

Uncertainty on yields in jets. The systematic uncertainty originating from the selection of the jet p_T were estimated by repeating the analysis with jet p_T varied around the chosen thresholds of 10 and 20 GeV$/c$ by 2 GeV$/c$. This variation accounts for jet resolution due to detector effects and the fluctuations of the event background density as reported in [19]. For jets with

$p_{\mathrm{T\,ch\,jet}} > 10$ GeV/c at low momenta ($p_{\mathrm{T}}^{\mathrm{V}^0} < 2$GeV/$c$) it reaches up to 10% while it is about 20% for jets of $p_{\mathrm{T\,ch\,jet}} > 20$ GeV/c. The uncertainty remains almost constant of about 5% for $p_{\mathrm{T}}^{\mathrm{V}^0} > 2$ GeV/c independently of the $p_{\mathrm{T\,ch\,jet}}$. **check numbers**

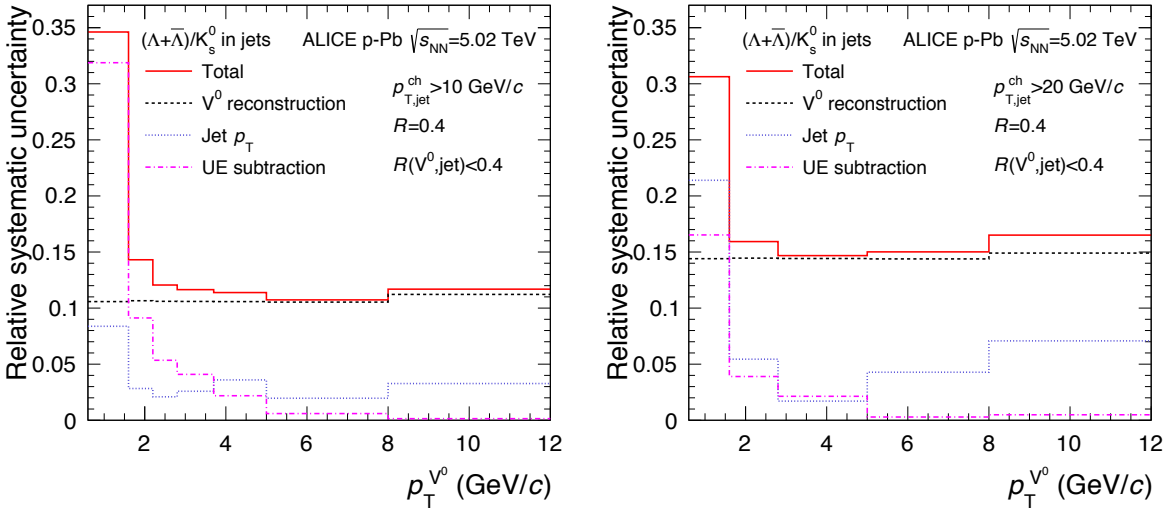

Fig. 3: Relative systematic uncertainty on the ratio of Λ and $\mathrm{K}^0_{\mathrm{S}}$ spectrum within $R = 0.4$ anti-k_{T} jets for $p_{\mathrm{T\,ch\,jet}} > 10\,\mathrm{GeV}/c$ (left) and $p_{\mathrm{T\,ch\,jet}} > 20\,\mathrm{GeV}/c$ (right) as a function of particle p_{T}. Three contributions to the total uncertainty are shown: uncertainty on V^0 reconstruction, uncertainty on the underlying event subtraction, and uncertainty on the jet momentum scale and momentum resolution.

Uncertainty on the $\Lambda/\mathrm{K}^0_{\mathrm{S}}$ ratio. The uncertainties on V^0 yields, material budget and feeddown correction are propagated to the ratio quadratically. The uncertainties related to the jet p_{T} and UE estimation are obtained by calculating the deviation of ratios between the default analysis and various selections. Figure 3 shows the relative systematic uncertainties on the $(\Lambda+\overline{\Lambda})/\mathrm{K}^0_{\mathrm{S}}$ ratio reconstructed within $R = 0.4$ jets with $p_{\mathrm{T\,ch\,jet}} > 10$ GeV/c and $p_{\mathrm{T\,ch\,jet}} > 20$ GeV/c as a function of particles p_{T}. For the $p_{\mathrm{T\,ch\,jet}} > 20$ GeV/c the total uncertainty is about 16% and is largely independent of particle p_{T} with the largest contribution of 14% originating from the uncertainty on V^0 reconstruction.

3 Results

3.1 p_{T} dependent strange particle densities

The fully corrected densities of $\mathrm{K}^0_{\mathrm{S}}$ and the sum of Λ and $\overline{\Lambda}$ particles associated to a hard scattering tagged by a jet are shown in Fig. 4. The per jet density within the jet cone (JC) is compared to the density for inclusive particles (without association to jets) and to the density in the perpendicular cones (PC). In the case of inclusive particles the distribution is normalized to the product of the total number of events and the acceptance of the V^0 particles in a single event (full azimuth and $|\eta| < 0.75$). As expected, for both $\mathrm{K}^0_{\mathrm{S}}$ and Λ particles the density within jets is much harder as the high-p_{T} particles originate from jets. The density in the PC selection is qualitatively similar to the inclusive distribution showing strong p_{T} dependence. Both, the inclusive and the PC distributions show a rapid decrease with p_{T} reaching values more than

an order of magnitude lower than the JC density for particle p_{T} exceeding 4 GeV/c. This is consistent with an expectation that the high-p_{T} particles originate from jet fragmentation.

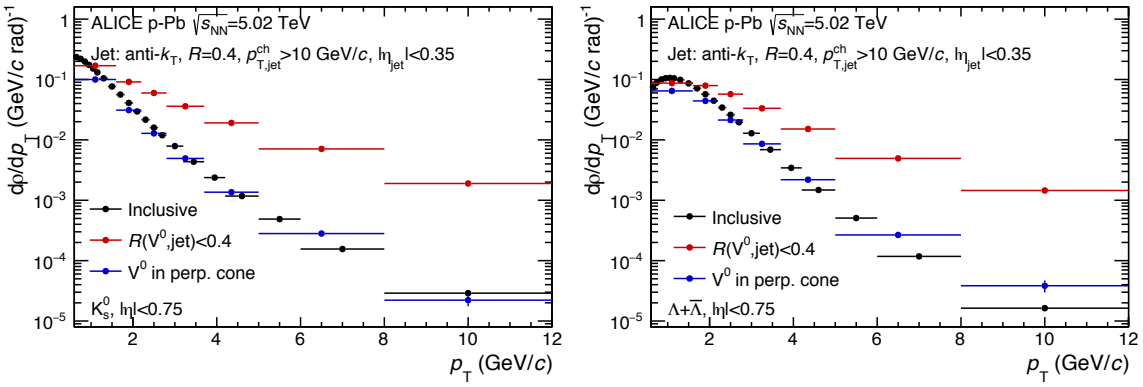

Fig. 4: Differential density of particles $\mathrm{d}\rho^{\mathrm{V}^0}/\mathrm{d}p_{\mathrm{T}}$ (see Eq. 2) in p-Pb collisions at $\sqrt{s_{\mathrm{NN}}} = 5.02$ TeV for $\mathrm{K}^0_{\mathrm{S}}$ (left), and the sum of Λ and $\overline{\Lambda}$ (right). The density is shown for three selections: inclusive particles from minimum bias events, particles within a anti-k_{T} jet ($p_{\mathrm{T\,ch\,jet}} > 10$ GeV/c) with $R = 0.4$ and the perpendicular cones (PC) in events containing the jet.

3.2 $(\Lambda+\overline{\Lambda})/\mathrm{K}^0_{\mathrm{S}}$ ratios

Ratios of Λ and $\mathrm{K}^0_{\mathrm{S}}$ yields can be obtained by dividing the normalized density distributions. In the following the sum of Λ and $\overline{\Lambda}$ densities is divided by twice the density of $\mathrm{K}^0_{\mathrm{S}}$. As no significant difference was found for different jet resolution parameters R the results are presented as the average of results obtained with R of 0.2, 0.3, and 0.4. Figure 5 shows the ratio for the raw JC selection (JC yield without the UE background subtraction) as a function of the distance from the jet axis $R(\mathrm{V}^0,jet)$. The ratio is shown for three momentum bins: the low-p_{T} ($0.6 < p_{\mathrm{T}} < 1.8$ GeV/c), intermediate p_{T} ($2.2 < p_{\mathrm{T}} < 3.7$ GeV/c), and the high-p_{T} ($4.2 < p_{\mathrm{T}} < 12$ GeV/c). The ratio as a function of $R(\mathrm{V}^0,jet)$ at low-p_{T} remains approximately constant at about 0.2 independent of the distance to the jet axis and that is the case even at large distances of $R(\mathrm{V}^0,jet) > 1.2$. This value is consistent with the inclusive measurements in p–Pb collisions, but also in pp and peripheral Pb–Pb collisions were effects related to the collective expansion of the system are either not-present or small [47].

Conversely the intermediate-p_{T} selection shows an increase of the ratio from about 0.3 when evaluated close to the jet axis to values of about 0.6 at $R(\mathrm{V}^0,jet)$ distances of about 0.5. For distances $R(\mathrm{V}^0,jet) > 0.5$ the ratio remains constant. The ratio of 0.6 is consistent with the inclusive measurement in p–Pb collisions [15] and this p_{T} region is where the ehnanced $\Lambda/\mathrm{K}^0_{\mathrm{S}}$ ratio in the inclusive measurements was found the largest. We stress that for the results shown in Fig. 5 the UE backgrounds were not subtracted. Therefore the evolution of the ratio as a function of the distance from the axis demonstrates how the two sources UE and jet compete. The lack of enhancement (values consistent with pp collisions) close to the jet axis indicate that the enhanced $\Lambda/\mathrm{K}^0_{\mathrm{S}}$ ratio is not associated with the jets.

In each of the momentum bins the ratio is dominated by the lower edge of the selection window due to steeply falling particle p_{T} spectrum. This is especially the case for the high-p_{T} selection where the dominating component originates from p_{T} of about 4.5 GeV/c and the $R(\mathrm{V}^0,jet)$ dependence at high-p_{T} is similar to intermediate p_{T}. The ratio at high-p_{T} accociated to jets is discussed below.

The right panel of Fig.5 shows the ratio of Λ to K^0_S as a function of particle p_T for four selections: the inclusive particles, the particles from the PC selection, and two JC selections for jet p_T of 10 and 20 GeV/c averaged over three resolution parameters R (0.2, 0.3, 0.4). In this case JC selection, prior to forming the ratio, the UE density contribution obtained with the PC selection was subtracted for each particle species separately. Additionally, for the results in Fig. 5 every V^0 particle was required to be close to the jet axis with its distance $R(V^0,jet) < 0.2$. The inclusive and the PC distributions show the enhancement at p_T of about 3 GeV/c. The ratio for the inclusive case is consistent with the measurement presented in [15]. The PC distribution above 2 GeV/c reaches systematically higher values than the inclusive. The $(\Lambda+\overline{\Lambda})/K^0_S$ ratio within jets is consistently lower than the inclusive case and approximately independent of p_T beyond 2 GeV/c. In particular, the ratio for particles associated to the jet does not show a maximum at the intermediate p_T. Clearly the enhancement of the ratio seen in the inclusive measurement is not present within jets. This conclusion holds for both, 10 GeV/c but also higher p_T (20 GeV/c) jets.

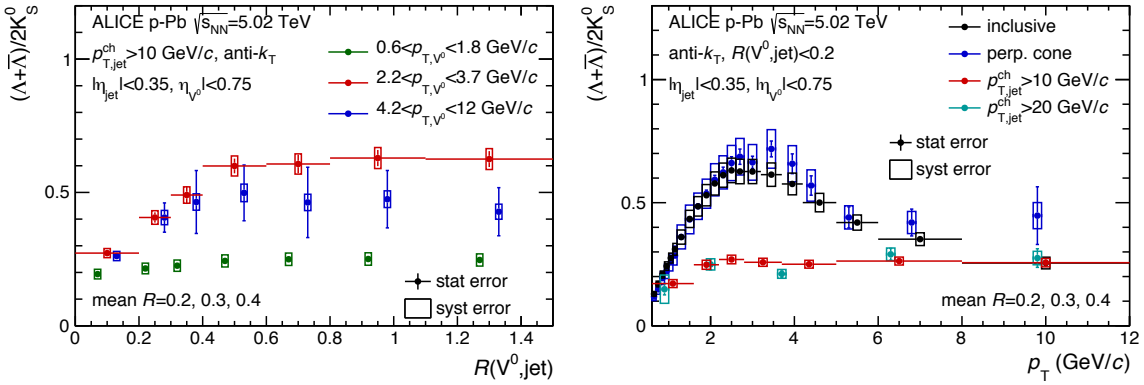

Fig. 5: Λ/K^0_S ratio in p-Pb collisions at $\sqrt{s_{NN}} = 5.02$ TeV as a function of R_{V^0-jet} for three different V^0-particle p_T selections associated with charged jets with $p_{T\,ch\,jet} > 10$ GeV/c (left) and as a function of V^0-particle p_T associated with charged jets with pT $p_{T\,ch\,jet} > 10$ GeV/c and 20 GeV/c together with that in inclusive and PC distribution (right). For more details see legend.

3.3 Discussion

the following is to be reworked or removed all together - it is a comment and not altering any of the conclusions:

Selecting hard scatterings according to the jet energy carried exclusively by the primary charged particles induces biases and inefficiencies in selection of the parton showers. The bias is related to the probabilistic process of fragmentation and hadronization. The analysis presented here tags only parton showers that fragmented into a configuration of hadrons that produce $p_{T\,ch\,jet} >$ 10 GeV/c charged particle jet with a given R with a finite efficiency. Therefore, there can be cases of V^0 particles that originated from a parton shower but were rejected in the analysis based on the energy carried only by the primary charged particles. The same analysis performed using PYTHIA event generator shows that the most probable p_T of the full jet with $R = 0.4$ is larger by about 40% as compared to the $p_{T\,ch\,jet}$. Moreover, since the daughters of the V^0 particles are not included in the jet energy calculation there are cases of jets containig V^0 particles but not included in the JC selection. On the other hand, the right panel of Fig. 5 shows that the inclusive Λ/K^0_S ratio at high-p_T is fully consistent with the ratio from particles associated to jets in this analysis. This hints that the conclusion on the absence of the baryon/meson

enhancement in jets made with the charged jets alone holds for all energetic parton showers and hadron configurations within jets.

4 Summary

In conclusion, the enhancement in the $(\Lambda+\overline{\Lambda})/\mathrm{K}^0_\mathrm{S}$ ratio found in the p–Pb and Pb–Pb collisions is not present in p–Pb for particles associated to a hard scattering taged by jets reconstructed from charged particles for $p_{\mathrm{T\,ch\,jet}} > 10$ GeV/c. This conclusion is consistent with the measurements in Pb–Pb collisions were the relative fragmentation into hadrons at high-p_T, even in central collisions, is not modified by the medium [16, 48, 49]. Moreover, as the baryon/meson enhancement has been linked to the interplay of radial flow and parton recombination at intermediate-p_T its absence within the jet cone demonstrates that these effects are limited to the soft processes of particle production.

Acknowledgements

References

[1] H. Satz, "Color deconfinement in nuclear collisions," *Rept.Prog.Phys.* **63** (2000) 1511, arXiv:hep-ph/0007069 [hep-ph].

[2] S. Bass, M. Gyulassy, H. Stoecker, and W. Greiner, "Signatures of quark gluon plasma formation in high-energy heavy ion collisions: A Critical review," *J.Phys.* **G25** (1999) R1–R57, arXiv:hep-ph/9810281 [hep-ph].

[3] E. V. Shuryak, "THEORY AND PHENOMENOLOGY OF THE QCD VACUUM. 7. MACROSCOPIC EXCITATIONS," *Phys.Rept.* **115** (1984) 151.

[4] J. Cleymans, R. Gavai, and E. Suhonen, "Quarks and Gluons at High Temperatures and Densities," *Phys.Rept.* **130** (1986) 217.

[5] S. Borsanyi, G. Endrodi, Z. Fodor, A. Jakovac, S. D. Katz, *et al.*, "The QCD equation of state with dynamical quarks," *JHEP* **1011** (2010) 077, arXiv:1007.2580 [hep-lat].

[6] T. Bhattacharya, M. I. Buchoff, N. H. Christ, H.-T. Ding, R. Gupta, *et al.*, "QCD Phase Transition with Chiral Quarks and Physical Quark Masses," *Phys.Rev.Lett.* **113** no. 8, (2014) 082001, arXiv:1402.5175 [hep-lat].

[7] B. Muller and J. L. Nagle, "Results from the relativistic heavy ion collider," *Ann.Rev.Nucl.Part.Sci.* **56** (2006) 93–135, arXiv:nucl-th/0602029 [nucl-th].

[8] E. Schnedermann, J. Sollfrank, and U. W. Heinz, "Thermal phenomenology of hadrons from 200-A/GeV S+S collisions," *Phys.Rev.* **C48** (1993) 2462–2475, arXiv:nucl-th/9307020 [nucl-th].

[9] **CMS** Collaboration, V. Khachatryan *et al.*, "Observation of Long-Range Near-Side Angular Correlations in Proton-Proton Collisions at the LHC," *JHEP* **1009** (2010) 091, arXiv:1009.4122 [hep-ex].

[10] **CMS** Collaboration, S. Chatrchyan *et al.*, "Observation of long-range near-side angular correlations in proton-lead collisions at the LHC," *Phys.Lett.* **B718** (2013) 795–814, arXiv:1210.5482 [nucl-ex].

[11] **ALICE** Collaboration, B. Abelev *et al.*, "Long-range angular correlations on the near and away side in p-Pb collisions at $\sqrt{s_{NN}} = 5.02$ TeV," *Phys. Lett.* **B719** (2013) 29–41, arXiv:1212.2001 [nucl-ex].

[12] **ATLAS** Collaboration, G. Aad *et al.*, "Observation of Associated Near-Side and Away-Side Long-Range Correlations in $\sqrt{s_{NN}}$=5.02 TeV Proton-Lead Collisions with the ATLAS Detector," *Phys.Rev.Lett.* **110** no. 18, (2013) 182302, arXiv:1212.5198 [hep-ex].

[13] **ATLAS** Collaboration, G. Aad *et al.*, "Measurement with the ATLAS detector of multi-particle azimuthal correlations in p+Pb collisions at $sqrt(s_{NN})$=5.02 TeV," *Phys.Lett.* **B725** (2013) 60–78, arXiv:1303.2084 [hep-ex].

[14] **CMS** Collaboration, S. Chatrchyan *et al.*, "Multiplicity and transverse momentum dependence of two- and four-particle correlations in pPb and PbPb collisions," *Phys.Lett.* **B724** (2013) 213–240, arXiv:1305.0609 [nucl-ex].

[15] **ALICE** Collaboration, B. B. Abelev *et al.*, "Multiplicity Dependence of Pion, Kaon, Proton and Lambda Production in p-Pb Collisions at $\sqrt{s_{NN}}$ = 5.02 TeV," *Phys. Lett.* **B728** (2014) 25–38, arXiv:1307.6796 [nucl-ex].

[16] **ALICE** Collaboration, B. B. Abelev *et al.*, "K^0_S and Λ production in Pb-Pb collisions at $\sqrt{s_{NN}}$ = 2.76 TeV," *Phys. Rev. Lett.* **111** (2013) 222301, arXiv:1307.5530 [nucl-ex].

[17] **ALICE** Collaboration, B. B. Abelev *et al.*, "Long-range angular correlations of π, K and p in p-Pb collisions at $\sqrt{s_{\rm NN}}$ = 5.02 TeV," *Phys. Lett.* **B726** (2013) 164–177, arXiv:1307.3237 [nucl-ex].

[18] R. Fries, B. Muller, C. Nonaka, and S. Bass, "Hadronization in heavy ion collisions: Recombination and fragmentation of partons," *Phys.Rev.Lett.* **90** (2003) 202303, arXiv:nucl-th/0301087 [nucl-th].

[19] **ALICE** Collaboration, J. Adam *et al.*, "Measurement of charged jet production cross sections and nuclear modification in p-Pb collisions at $\sqrt{s_{\rm NN}} = 5.02$ TeV," *Phys. Lett.* **B749** (2015) 68–81, arXiv:1503.00681 [nucl-ex].

[20] **ALICE** Collaboration, J. Adam *et al.*, "Measurement of dijet k_T in p-Pb collisions at $\sqrt{s}_{NN}$=5.02 TeV," *Phys. Lett.* **B746** (2015) 385–395, arXiv:1503.03050 [nucl-ex].

[21] L. D. McLerran, "The Color glass condensate and small x physics: Four lectures," *Lect.Notes Phys.* **583** (2002) 291–334, arXiv:hep-ph/0104285 [hep-ph].

[22] C. Salgado, J. Alvarez-Muniz, F. Arleo, N. Armesto, M. Botje, *et al.*, "Proton-Nucleus Collisions at the LHC: Scientific Opportunities and Requirements," *J.Phys.* **G39** (2012) 015010, arXiv:1105.3919 [hep-ph].

[23] A. Krzywicki, J. Engels, B. Petersson, and U. Sukhatme, "Does a Nucleus Act Like a Gluon Filter?," *Phys.Lett.* **B85** (1979) 407.

[24] A. Accardi, "Final state interactions and hadron quenching in cold nuclear matter," *Phys.Rev.* **C76** (2007) 034902, arXiv:0706.3227 [nucl-th].

[25] **ATLAS** Collaboration, G. Aad *et al.*, "Observation of a Centrality-Dependent Dijet Asymmetry in Lead-Lead Collisions at $\sqrt{s_{NN}} = 2.77$ TeV with the ATLAS Detector at the LHC," *Phys.Rev.Lett.* **105** (2010) 252303, arXiv:1011.6182 [hep-ex].

[26] **CMS** Collaboration, S. Chatrchyan *et al.*, "Jet momentum dependence of jet quenching in PbPb collisions at $\sqrt{s_{NN}} = 2.76$ TeV," *Phys.Lett.* **B712** (2012) 176–197, arXiv:1202.5022 [nucl-ex].

[27] **ATLAS** Collaboration, G. Aad *et al.*, "Measurement of the jet radius and transverse momentum dependence of inclusive jet suppression in lead-lead collisions at $\sqrt{s_{NN}}$= 2.76 TeV with the ATLAS detector," *Phys.Lett.* **B719** (2013) 220–241, arXiv:1208.1967 [hep-ex].

[28] **ALICE** Collaboration, B. Abelev *et al.*, "Measurement of charged jet suppression in Pb-Pb collisions at $\sqrt{s_{NN}}$ = 2.76 TeV," *JHEP* **03** (2014) 013, arXiv:1311.0633 [nucl-ex].

[29] **ATLAS** Collaboration, G. Aad *et al.*, "Measurements of the Nuclear Modification Factor for Jets in Pb+Pb Collisions at $\sqrt{s_{\rm NN}} = 2.76$ TeV with the ATLAS Detector," *Phys.Rev.Lett.* **114** no. 7, (2015) 072302, arXiv:1411.2357 [hep-ex].

[30] **ALICE Collaboration** Collaboration, K. Aamodt *et al.*, "The ALICE experiment at the CERN LHC," *JINST* **3** (2008) S08002.

[31] L. Evans and P. Bryant, "LHC Machine," *JINST* **3** (2008) S08001.

[32] **ALICE** Collaboration, E. Abbas *et al.*, "Performance of the ALICE VZERO system," *JINST* **8** (2013) P10016, arXiv:1306.3130 [nucl-ex].

[33] **ALICE** Collaboration, B. Abelev *et al.*, "Pseudorapidity density of charged particles in p + Pb collisions at $\sqrt{s_{NN}} = 5.02$ TeV," *Phys. Rev. Lett.* **110** no. 3, (2013) 032301, arXiv:1210.3615 [nucl-ex].

[34] A. Akindinov, A. Alici, A. Agostinelli, P. Antonioli, S. Arcelli, *et al.*, "Performance of the ALICE Time-Of-Flight detector at the LHC," *Eur.Phys.J.Plus* **128** (2013) 44.

[35] **ALICE** Collaboration, K. Aamodt *et al.*, "Alignment of the ALICE Inner Tracking System with cosmic-ray tracks," *JINST* **5** (2010) P03003, arXiv:1001.0502 [physics.ins-det].

[36] J. Alme, Y. Andres, H. Appelshauser, S. Bablok, N. Bialas, *et al.*, "The ALICE TPC, a large 3-dimensional tracking device with fast readout for ultra-high multiplicity events," *Nucl.Instrum.Meth.* **A622** (2010) 316–367, arXiv:1001.1950 [physics.ins-det].

[37] M. Cacciari, G. P. Salam, and G. Soyez, "The Anti-k(t) jet clustering algorithm," *JHEP* **0804** (2008) 063, arXiv:0802.1189 [hep-ph].

[38] M. Cacciari, G. P. Salam, and G. Soyez, "FastJet User Manual," *Eur.Phys.J.* **C72** (2012) 1896, arXiv:1111.6097 [hep-ph].

[39] M. Cacciari and G. P. Salam, "Dispelling the N^3 myth for the k_t jet-finder," *Phys.Lett.* **B641** (2006) 57–61, arXiv:hep-ph/0512210 [hep-ph].

[40] M. Cacciari, G. P. Salam, and G. Soyez, "The Catchment Area of Jets," *JHEP* **0804** (2008) 005, arXiv:0802.1188 [hep-ph].

[41] **ALICE** Collaboration, J. Adam *et al.*, "Measurement of jet suppression in central Pb-Pb collisions at $\sqrt{s_{\rm NN}}$ = 2.76 TeV," *Phys. Lett.* **B746** (2015) 1–14, arXiv:1502.01689 [nucl-ex].

[42] T. Sjostrand, S. Mrenna, and P. Z. Skands, "A Brief Introduction to PYTHIA 8.1," *Comput. Phys. Commun.* **178** (2008) 852–867, arXiv:0710.3820 [hep-ph].

[43] **ALICE** Collaboration, B. B. Abelev *et al.*, "Performance of the ALICE Experiment at the CERN LHC," *Int. J. Mod. Phys.* **A29** (2014) 1430044, arXiv:1402.4476 [nucl-ex].

[44] **Particle Data Group** Collaboration, B. D. Fields, P. Molaro, and S. Sarkar, "Big-bang nucleosynthesis," *Chin.Phys.* **C38** (2014) 090001, arXiv:1412.1408 [astro-ph].

[45] S. Roesler, R. Engel, and J. Ranft, "The Monte Carlo event generator DPMJET-III," arXiv:hep-ph/0012252 [hep-ph].

[46] **ALICE** Collaboration, B. Abelev *et al.*, "Multi-strange baryon production in pp collisions at $\sqrt{s} = 7$ TeV with ALICE," *Phys. Lett.* **B712** (2012) 309–318, arXiv:1204.0282 [nucl-ex].

[47] **ALICE** Collaboration, B. B. Abelev *et al.*, "$K^*(892)^0$ and $\phi(1020)$ production in Pb-Pb collisions at $\sqrt{sNN}$ = 2.76 TeV," *Phys. Rev.* **C91** (2015) 024609, arXiv:1404.0495 [nucl-ex].

[48] **ALICE** Collaboration, B. B. Abelev *et al.*, "Production of charged pions, kaons and protons at large transverse momenta in pp and Pb-Pb collisions at $\sqrt{s_{\rm NN}}$ =2.76 TeV," *Phys. Lett.* **B736** (2014) 196–207, arXiv:1401.1250 [nucl-ex].

[49] **ALICE** Collaboration, J. Adam *et al.*, "Centrality dependence of the nuclear modification factor of charged pions, kaons, and protons in Pb-Pb collisions at $\sqrt{s_{\rm NN}} = 2.76$ TeV," *Phys. Rev.* **C93** no. 3, (2016) 034913, arXiv:1506.07287 [nucl-ex].

A The ALICE Collaboration